REALIZABILITY AND STABILITY ANALYSIS OF DYNAMIC LES

Reza Mokhtarpoor

Department of Mathematics
University of Wyoming
1000 E. Univ. Ave., Laramie WY 82071, USA
rmokhtar@uwyo.edu

Stefan Heinz

Department of Mathematics
University of Wyoming
1000 E. Univ. Ave., Laramie WY 82071, USA
heinz@uwyo.edu

Michael Stoellinger

Department of Mechanical Engineering
University of Wyoming
1000 E. Univ. Ave., Laramie WY 82071, USA
mstoell@uwyo.edu

ABSTRACT

Our original dynamic LES subgrid-scale (SGS) model was obtained on the basis of a realizable stochastic model for turbulent velocities. However, realizablity of PDF equations does not necessarily ensure the full realizability of a SGS model. By analyzing the structure of the SGS stress tensor we have derived a condition for the realizibility of the SGS stress tensor which makes our original dynamic DGS model fully realizable. The corresponding dynamic bounds are applicable to any SGS model which has an eddy viscosity structure. It is found that stress-realizablility ensures stability, whereas a model that is not stress-realizable can become unstable. Extensive investigations are carried out for studying the reason of instabilities in dynamic SGS models. It is found that instabilities in dynamic SGS models are produced by imbalances originated via large gradients of the standard deviations of dynamic model parameters.

INTRODUCTION

One of the most interesting features developed in large eddy simulation is the dynamic subgrid-scale procedure. It is a general method for calculation of model constants as a function of time and space as the simulation progresses. This helps us to avoid any treatment of model constant (e.g., damping or wall modeling) near the wall boundaries. Although dynamic SGS models are extremely attractive, but they suffer from instabilities. The principal reason that why the SGS models have such an unstable property has not yet been fully clarified.

The first step to avoid instability could be developing a realizable SGS model. Heinz developed a dynamic SGS model based on realizable stochastic model for turbulent velocities (Heinz, 2007). In applying this realizable model for different flows we found that the model can suffer from instability for some flows. For stabilization of the model we used to clip some negative values of C_S. We found that the realizibility of PDF equations does not necessarily ensure the realizability of SGS stress tensor. In this paper we introduced a method for stabilization of any SGS model that uses the Boussinesq hypothesis. By examining the structure of the SGS stress tensor we derived a condition for realizibility of SGS stress tensor. By applying this condition to our original model we made our model strongly stable for wide range of CFL number. Then, extensive investigations are performed for discovering the instability reason in a dynamic SGS model.

The paper is organized as following. First, we will consider the realizability of model from two approaches; realizability of PDF equations and realizibility of stress tensor. Second, we will derive a condition for realizibility of stress tensor. Third, we will described the flow considered for testing our method. Next, We will perform extensive stability analysis. Finally, the conclusions are summarized.

MODELING APPROACH

Realizability via Stochastic Analysis

The LES model is based on a realizable stochastic model for turbulent velocities proposed by Heinz (Heinz, 2003*a*,*b*, 2007, 2008; Heinz & Gopalan, 2012; Gopalan *et al.*, 2013). This model implies the exact but unclosed filtered Navier-Stokes equations.

Realizability via Stress Structure

Let us consider now realizability conditions that arise from the structure of the SGS stress tensor. Before doing so, we would like to refer to two facts. First, in line with the consideration of incompressible flow in this paper we will present this analysis for incompressible flow. However, the extension to compressible flow is simple: it just needs to replace $\widetilde{S}_{ij}$ by its deviatoric component $\widetilde{S}^d_{ij}$, and, correspondingly, $|\widetilde{S}|$ by $|\widetilde{S}^d|$. Second, the analysis presented in this subsection does not make any other assumption than the structure of τ_{ij} given above for the SGS stress. In particular, we do not assume any specific structure of the turbulent viscosity ν_t, this means our analysis results are applicable to all SGS stress models that use the SGS stress given above.

The SGS stress tensor τ_{ij} is a positive semi-definite matrix if it satisfies

$$\tau_{ij} \geq 0 \qquad for \qquad i = j, \tag{1}$$

$$\tau_{ij}^2 \leq \tau_{ii}\tau_{jj} \qquad for \qquad i \neq j, \tag{2}$$

$$det(\tau_{ij}) \geq 0. \tag{3}$$

We can use the first two conditions to obtain the following three realizability requirements for the SGS stress tensor,

$$\tau_{11} + \tau_{22} + \tau_{33} = 2k \geq 0, \tag{4}$$

$$\tau_{12}^2 + \tau_{13}^2 + \tau_{23}^2 \leq \tau_{11}\tau_{22} + \tau_{11}\tau_{33} + \tau_{22}\tau_{33}, \tag{5}$$

$$det(\tau_{ij}) \geq 0. \quad (6)$$

The SGS stress tensor is assumed to have an eddy viscosity structure given above. We introduce the nondimensional turbulent viscosity

$$\nu_t^* = \frac{\sqrt{3}}{2}\frac{\nu_t|\widetilde{S}|}{k}. \quad (7)$$

Then, it can be shown that all three realizability conditions are satisfied if $|\nu_t^*| \leq 0.47917 = 23/48$.

LES Models Considered

The closure of kinetic energy equation still requires the definition of the SGS viscosity ν_t. The combination of $\nu_t = k\tau_L/3$ with $\tau_L = 2(1-c_0)\Delta k^{-1/2}$, see above, implies the deterministic SGS model

$$\nu_t = \frac{2(1-c_0)}{3}k^{1/2}\Delta. \quad (8)$$

An equilibrium version of this SGS model can be obtained in the following way. According to kinetic energy equation, we equate the last two terms, this means we assume that the production is balanced by the dissipation. This implies

$$k^{1/2} = \sqrt{\frac{2(1-c_0)}{3}}\Delta|\widetilde{S}|. \quad (9)$$

By using this expression we obtain an equilibrium deterministic SGS stress model given by

$$\nu_t = \left[\frac{2(1-c_0)}{3}\right]^{3/2}\Delta^2|\widetilde{S}|. \quad (10)$$

The use of $c_0 = 0.86$ implies $\nu_t = 0.093k^{1/2}\Delta$ and $\nu_t = 0.17^2\Delta^2|\overline{S}|$ for the non-equilibrium and equilibrium SGS stress models. These settings correspond to standard models applied in several simulations. However, to avoid the need for any such SGS model parameter settings, dynamic versions of these LES models will be considered in the following.

Our first model considered, which will be referred to as noneqilibrium LDM (LDMK), applies the expression $\nu_t = C_S k^{1/2}\Delta$, where C_S is obtained via

$$C_S = -\frac{L_{ij}^d M_{ji}}{M_{kl}M_{lk}}. \quad (11)$$

Here, L_{ij}^d refers to the deviatoric component of the Leonard stress $L_{ij} = \widetilde{\widetilde{U}_i\widetilde{U}_j} - \widetilde{\widetilde{U}_i}\,\widetilde{\widetilde{U}_j}$ (the overbar refers to the test filter operation), and M_{ij} is given by

$$M_{ij} = 2\Delta^T\sqrt{k^T}\,\widetilde{\overline{S}}_{ij}, \quad (12)$$

which involves the test-filter turbulent kinetic energy $k^T = L_{nn}/2$ and filter width on the test-filter level $\Delta^T = 2\Delta$.

Our second model considered is the original dynamic Smagorinsky model (DSM), which does not involve any averaging or clipping of dynamic model coefficients. This model applies an equilibrium expression for k in the SGS viscosity ν_t leading to $\nu_t = C_S\Delta^2|\widetilde{S}|$, where C_S is obtained via

$$C_S = -\frac{L_{ij}^d H_{ij}}{H_{mn}H_{mn}}, \quad (13)$$

where the expression H_{ij} is given by

$$H_{ij} = 2\left(\Delta^T\right)^2|\widetilde{\overline{S}}|\widetilde{\overline{S}}_{ij} - 2\Delta^2\overline{|\widetilde{S}|\widetilde{S}_{ij}}. \quad (14)$$

Combination of LES Models with Bounds

According to the realizability condition $|\nu_t^*| \leq 23/48$ derived in the previous subsection, we find the following C_S realizability condition for the LDMK is given by

$$|C_S| \leq \frac{23}{24\sqrt{3}}\frac{k^{1/2}}{\Delta|\widetilde{S}|}, \quad (15)$$

and the realizability condition for the DSM model is given by

$$|C_S| \leq \frac{23}{24\sqrt{3}}\frac{k}{\Delta^2|\widetilde{S}|^2}. \quad (16)$$

The problem with using Eq. (16) in conjunction with the DSM is that k is not available by using these methods. One of the options is to approximate k by Yoshizawa's expression (Yoshizawa, 1986), $k = C_I\Delta^2|\tilde{S}|^2$, where C_I is given by $C_I = k^T/((\Delta^T)^2|\widetilde{\overline{S}}|^2)$. Here C_I is obtained by the approximation $L_{kk}/2 = k^T = C_I(\Delta^T)^2|\tilde{S}|^2$. Similar method is used by (Moin *et al.*, 1991). We found that this formula is just an approximation for k and it is not a good approximation everywhere; therefor we would use a coefficient C_k in the following bound formula

$$|C_S| \leq \frac{23C_k}{24\sqrt{3}}\frac{k^T}{(\Delta^T)^2|\widetilde{\overline{S}}|^2}, \quad (17)$$

as realizibility bound for DSM. The use of DSM in conjunction with Eq. (17), where C_k has to be determined from simulations, will be referred to as DSMS.

COMPUTATIONAL DETAILS

We considered separated flow over two-dimensional hills. This flow configuration creates a variety of relevant flow features such as separation, recirculation, and natural reattachment. It follows the numerical work of Mellen *et al.* (2000). This geometry has been used for various numerical studies and served as a benchmark for testing the performance of various turbulence models.

Figure 1 shows the computational domain applied in our simulations. The size of the computational domain is $L_x = 9h$, $L_y = 3.035h$, and $L_z = 4.5h$ in streamwise (x), wall normal (y), and spanwise (z) directions, respectively, where h is the height of the hill. The hill crest is located at $(x,y)/h = (0,1)$. The Reynolds number $Re = U_b h/\nu$ is $Re = 37{,}000$ based on the hill height and bulk velocity above the hill crest at $x = 0$. At the bottom and top, the channel is constrained by solid walls. No-slip and impermeability boundary conditions are used at these walls. Periodic boundary conditions are employed in streamwise and spanwise directions. In

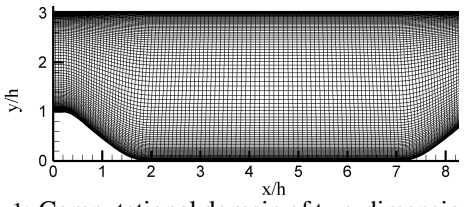

Figure 1: Computational domain of two-dimensional hill flow simulations: the reference curvilinear grid is shown.

recently published paper (Mokhtarpoor *et al.*, 2016) we investigated the same flow using pure LES and also unified RANS-LES models. We also studied grid effect for both models for grids ranging from 60 K to 20 M cells. In present study, our aim is to analyze

the stability of dynamic models by investigating the effect of different parameters. Therefore we will use a reference grid for all of our studies. From our previous studies we found that the grid of $N_x \times N_y \times N_z = 128 \times 80 \times 48$ with 500 K cells is a pretty logical mesh for present study.

Our computations are initialized by a uniform bulk velocity U_b except in cases in which we wanted to calculate correlation functions where we restarted our calculations with stationary solutions.

1 RESULTS A: LDMK

Although the original LDMK SGS model proposed by (Heinz, 2007) was based on a realizable stochastic model for turbulent velocities, but it does not necessarily ensure the realizibility of stress tensor. In applying the original LDMK model for different flows we found that for some flows the model suffers from instability if we do not use any clipping for negative values of the model constant, C_s. For stabilization of the model, we used to clip some negative values of C_s in the original LDMK model and referred to this model LDMK-CC (LDMK with constant clipping). This model will be discussed later in details.

By applying the realizability condition for structure of SGS stress tensor we made the new LDMK model fully realizable. To examine the realizibilty of the dynamic coefficient, C_s, we have monitored time histories of C_s using the new LDMK model. Figure 2 shows the time histories of C_s along with its realizibility bounds for two probe points during 30 flow-through times (FTTs). The location of probe point P1 is in the shear in top of the first hill and P2 is in downstream of P1 in middle of two hills. The red and blue circles in Fig. 2 indicate the times at which C_s values hit the upper and lower realizibilty bounds, respectively. In the probe point P1, we found that in 30 FTTs (corresponding to 150,000 iterations) in average 2 out 100 iterations C_s value hits the upper (positive) realiziblity bound, and about the same C_s value hits the lower (negative) realizibility bound. In the probe point P2, the frequency of hitting is about 4 out of 1000 iterations in average for both lower and upper bounds. This shows that the original LDMK model is almost a realizable model which is implied by its PDF-realizability but it is not fully realizable model, which sometimes for some flows give rise to instability. By using the SGS stress tensor realizibility conditions we have made the model fully realizable. Next, we study the effect of simulation time step in realizibility of the model.

For studying the effectiveness of these bounds on the stability of dynamic model we used another dynamic LDMK version which applies bounds that are 1.2, 1.5, and 2 times bigger than the regular bounds (see Eq. (15)). We refer to these model LDMK-1.2B, LDMK-1.5B and LDMK-2B, respectively. Table 1 summarizes the stability analysis results for LDMK and other extended bound versions. We called a model stable when it does not become unstable for 100 FTTs. We see that LDMK is strongly stable for wide range of time steps between $\Delta t = 10^{-3}$–10^{-2} which corresponds CFL numbers ranging between 0.1–0.9. But, the LDMK-1.2B is only stable for time steps $\Delta t = 0.001$ and 0.002 and the LDMK-1.5B and LDMK-2B are unstable even for small CFL number (small Δt). It can be concluded that: first, by applying realizability bound we made the LDMK model fully realizable; second, a model that is not stress-realizable can become unstable.

2 RESULTS B: STABILITY ANALYSIS

Dynamic model procedure is a method for determining the SGS model constant which makes the method attractive especially for flows in complex geometries where it is difficult to calibrate model constants. But, this procedure usually suffers from instability without using either averaging or clipping methods. It is known that by clipping of negative model constants which is not a favorable method we can avoid instability but we don't know the actual reason of how the model constants can cause the instability. In preceding section, we observed that even a PDF realizable dynamic model can locally produce model constants that is nonphysical (non-realizable). Number of occurrence of these local nonphysical events can be cause of the instability. Another potential reason could be the correlation of non-physical model constant. This can be happen in two different ways; when a SGS model produces a nonphysical model constant in a specific time and space this nonphysical event can be elongated in that specific point for a long time or it can be spread in space. Lund *et al.* (1993) claimed that instability of dynamic SGS model is mostly related to the time interval over which the negative model coefficient remains correlated. Another possibility is that when a SGS model produces nonphysical large positive and negative model constants, at the same time it brings about large gradients which numerical model can not handle it and give rise to instability. In some dynamic models positive total viscosity have been used for stabilization of models. Negative total viscosity in diffusion terms of momentum or turbulent kinetic energy can be a reason of instability.

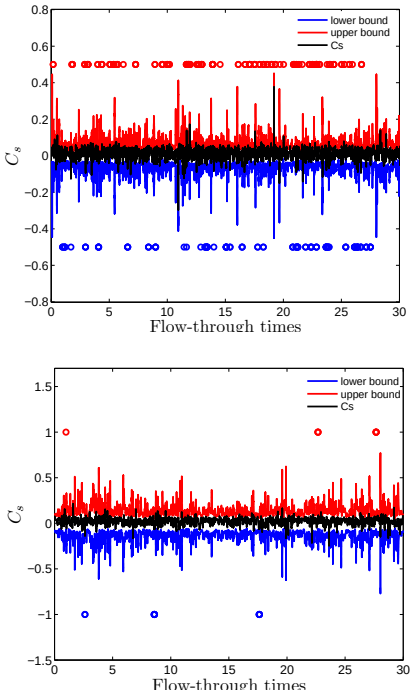

Figure 2: Time histories of C_s and its realizibility bounds in LDMK simulations for the last 30 flow-through times at two different probe points P1 (upper plot) and P2 (lower plot). The red and blue circles indicate the times at which C_s values hit the upper and lower realizibilty bounds, respectively. The time step is $\Delta t = 0.002$.

In the following, we will study the possible instability reasons in details. For investigating any possible reason, we will compare two stable and unstable models. Since LDMK-CC model with big negative clipping (e.g., $C_{clip} = -0.2$) is very unstable model in which instability happens in less than 5 FTTs we could clearly see the differences of stable and unstable cases. But we couldn't calculate the correlation functions in unstable LDMK-CC models because we needed reasonable samples for calculation of correlation function. Hence, only for studying the effect of correlations we will use unstable LDMK-2B model that instability happens after 56 FTTs.

Table 1: Stability analysis of LDMK and its extended bound versions at different time steps.

Simulation	$\Delta t = 0.001$	$\Delta t = 0.002$	$\Delta t = 0.004$	$\Delta t = 0.008$	$\Delta t = 0.01$
$LDMK$	Stable	Stable	Stable	Stable	Stable
$LDMK-1.2B$	Stable	Stable	Unstable	Unstable	Unstable
$LDMK-1.5B$	Unstable	Unstable	Unstable	Unstable	Unstable
$LDMK-2B$	Unstable	Unstable	Unstable	Unstable	Unstable

Effect of Correlations

One of the possible instability reasons could be the correlation of non-physical (non-realizable) model constants. This correlation can be in time and space. Lund *et al.* (1993) claimed that instability of dynamic SGS model is mainly due to the elongated negative model constants. In this study, we aimed to re-examine their conclusion. It is obvious that we should calculate the correlation function in a region where the occurrence of negative C_s is high. The time correlation function is calculated in two points, one of them is P3, located in the center of the bubble where we have largest occurrence of negative C_s and another point, P4, is located in shear layer where we have large gradients of flow field quantities.

The temporal auto-correlation function of C_s, $R(\tau)$, at specific time t_0 is calculated by

$$R(\tau) = \frac{\langle C_s'(t_0) C_s'(t_0+\tau)\rangle}{\langle C_s'(t_0) C_s'(t_0)\rangle}. \tag{18}$$

Here $C_s' = C_s - \langle C_s\rangle$ is the fluctuation of C_s at specific time. Temporal correlation functions are calculated for a stable LDMK and an unstable LDMK-2B models. Since for the calculation of correlation functions we needed reasonable number of independent samples, we had to use a unstable model which instability occurs after relatively long time. For LDMK-2B model (with $\Delta t = 0.002$ s) instability occurs after 56 FTTs which corresponds to about 560 seconds. Independent samples are taken in every successive 1.4 seconds, because the correlation time for the points P3 and P4 are $0.6s$ and $1.4s$ respectively. The total number of samples used in time correlation calculations are $400 \times 40 = 16,000$ samples.

Figure 3 shows the Temporal correlation function for LDMK and LDMK-2B. For both models correlation time for point P3 is $0.6s$ and for point P4 is $1.4s$. It shows that the stable and unstable models have same correlation of C_s and hence correlation of C_s can not be the cause of instability.

Frequencies of occurrence of local non-realizable events

It was shown that even a dynamic SGS model which is based on realizable stochastic model rarely produces non-physical (non-realizable) model constants. Now the question is how this non-realizable events possibly could give rise to instability. One immediate answer could be the number of occurrence of this non-physical events. It is found that, although non-realizible events of unstable model is much more than the stable model but this can not be the reason of instability. If we look at the probability of non-realizable events of the stable LDMK model with time step $\Delta t = 0.008$ (not shown here) we found that its non-realizable events are more than the unstable LDMK-CC model with time step $\Delta t = 0.002$. Therefore the frequencies of occurrence of non-realizable events itself can not be the reason of instability.

Imbalances originated by large fluctuations of C_s

Next, we will investigate the effect of C_s fluctuations on instability. Standard deviation is considered here as a quantity that reflects the characteristic of fluctuations. We compared the standard deviation of stable and unstable models. It is found that in contrast to stable models which have approximately constant standard deviation in time or at most involve only smooth transition of standard deviations, unstable models experience big temporal jumps in standard deviations. Big jumps in time result in large gradients of standard deviation in space which can give rise to instability of the numerical model. In the following we will discuss it in details.

For comparing the characteristic of fluctuations for stable and unstable models, two stable LDMK-CC ($C_{clip} = -0.02, -0.05$) models and one unstable LDMK-CC ($C_{clip} = -0.2$) model are considered. Figure 4 shows the time histories and standard deviation of C_s at probe point P3 from start to 3 FTTs (corresponds to 15,000 iterations). It should be noted that all three simulations are initialized with the same initial condition. In calculation of standard deviation, the mean could be computed in different ways. Since our purpose was to discover the reason of instability, we had to find out what happens close to the time of instability. Therefore, the standard deviation of C_s is calculated by moving time averaging method. The moving time window of 0.4 FTT (corresponds to 2,000 iterations) is used. In other words, the standard deviation at time t is calculated from the last 2,000 iterations. First, we compare two stable LDMK-CC models. Standard deviations becomes approximately stationary after 2.0 FTTs (corresponds to 10,000 iterations) for this two models. Standard deviation of LDMK-CC models with clipping constants of -0.02 and -0.05 are about 0.017 and 0.023, respectively at the time of 2.6 FTTs. If we look at the fluctuations in LDMK-CC ($C_{clip} = -0.05$) between $2.2-2.6$ we can find that in 0.4 FTT (2000 iterations) there are about 800 iterations that the absolute values of C_s are bigger than 0.02; 450 iterations in negative and 350 in positive fluctuations. Therefore, in LDMK-CC ($C_{clip} = -0.05$), amplitudes of 40% ($800/2000 = 0.4$) of fluctuations are bigger than 0.02. But, LDMK-CC ($C_{clip} = -0.02$) has about 220 iterations that their absolute values are bigger than 0.02 (all in positive fluctuations). It means that only 10% ($200/2000 = 0.10$) of fluctuations are bigger than 0.02. Hence, LDMK-CC ($C_{clip} = -0.05$) have 30% more large fluctuations than LDMK-CC ($C_{clip} = -0.02$); this gave rise to 35% standard deviation differences for these two models. Now, we compare two LDMK-CC ($C_{clip} = -0.05, -0.2$) models. It can be seen that LDMK-CC ($C_{clip} = -0.2$) becomes unstable after 2.6 FTTs. We see that standard deviation of C_s for unstable model is about the same of LDMK-CC ($C_{clip} = -0.05$) before 2.2 FTTs . Before this time, the number of iterations that their amplitudes are bigger than 0.05 are only 400 (out of 11,000 iterations) for LDMK-CC ($C_{clip} = -0.2$). This value for LDMK-CC ($C_{clip} = -0.05$) is 240 iterations. Therefore the number of large fluctuation in two models are not that different to make observable standard deviation differences till flow-through time 2.2. We see that after this time, series of big fluctuations with maximum amplitudes of 0.25 and 0.22 occurred. Since the clipping is not that restrict for this model, large

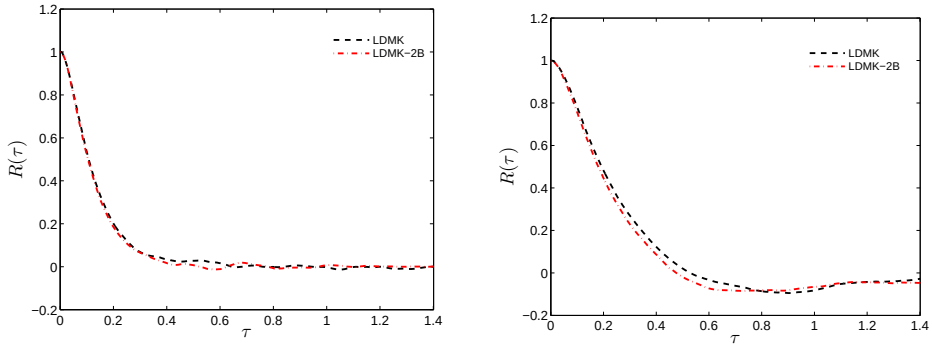

Figure 3: Temporal correlation function for LDMK and LDMK-2B at probe points P3 (left plot) and P4 (right plot). The time step $\Delta t = 0.002$.

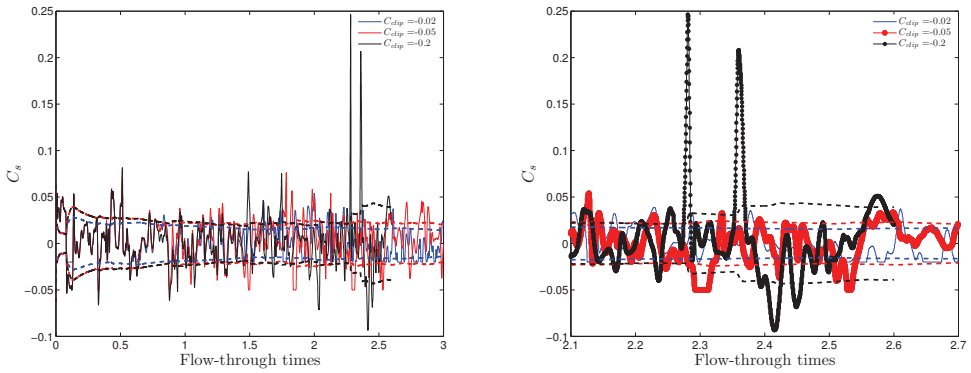

Figure 4: Time histories and standard deviation of C_s for LDMK-CC with three different clipping constants at probe point P3. Standard deviations are shown with dashed lines with the same color. The time step for both simulation is $\Delta t = 0.002$.

positive fluctuations are followed with large negative fluctuations as well. Between flow through time of 2.2 and 2.6 (which includes 2000 iterations) 300 iterations occur which their absolute amplitudes are bigger than 0.05. It should be noted till flow through times of 2.2 there is no fluctuation bigger than 0.08. But between $2.2-2.6$ there are about 160 events that absolute values of C_s are bigger than 0.08. The value of the standard deviation for unstable model reaches to 0.039 before the crash. We see that in contrast to stable models that have approximately constant standard deviations, the unstable model faced with about 70% increase in standard deviation of C_s between $2.2-2.6$ FTTs which ended up with the model instability. In addition, we see that unlike two stable models which standard deviations differences caused by large amount hitting of the bound in LDMK-CC ($C_{clip} = -0.02$), in the later case standard deviations differences caused by very large fluctuations (fluctuations that can be five times of 0.05). If we had more restrict clipping for unstable model, the fluctuations would be controlled after large positive fluctuations. For observing the instability reason in entire flow field, we look at the contour plots of standard deviation. Figure 5 (a, c and e) compares the contour plots of standard deviation of C_s for three models. Here again, it is shown that by decreasing the clipping constant, standard deviation of C_s increases. This increase is very significant in the unstable LDMK-CC model ($C_{clip} = -0.2$). The most important feature of the unstable LDMK-CC model is that the large fluctuations which are shown by red structures are not only increased but also spread in all the flow field. This is in consistent with Fig. 4 that shows instability occurs when standard deviation faces with abrupt changes in time. Because large jumps in time brings about large jumps in space as well. This causes the regions of high fluctuation get closer to regions that have relatively much smaller fluctuations (green and light blue) this can give rise to high gradients of magnitude of fluctuations in space. Figure 5 (b, d and f) compares the gradient of standard deviation of C_s in y direction for the same three models. It can be seen that in both stable LDMK-CC models large gradients of standard deviations (gradients of large fluctuations) happen near the upper and lower wall where the transition of very small to medium fluctuations happens. Note that the positive and negative values in upper and lower walls are related to direction of y axis and wall normal directions for the two walls. In contrast to the stable models, in the unstable model large gradients of fluctuations spreads in the regions that small to very large fluctuations of model constant have to be exist. It seems that the instability occurs in a model that produces non-physical (non-realizable) big C_s values that results in big fluctuation in time in all of the region. This cause regions with very small fluctuations get close to regions with very large fluctuations which produces large gradients of fluctuations (large imbalances) in space that can no longer be handled by numerical method and finally end up with unstable model.

CONCLUSIONS

The original PDF-realizable LDMK model was not fully realizable. This could cause instabilities in simulation of some flows. We used to apply clipping method for the stabilization of model. Then we found that the realizibility of PDF equations does not necessarily ensure the realizability of SGS stress tensor. By analyzing the structure of SGS stress tensor we have derived a condition for realizibility of SGS stress tensor which made the LDMK model fully realizable. Stability analysis performed on a high Reynolds number separated flow shows that the new fully realizible LES model, LDMK,

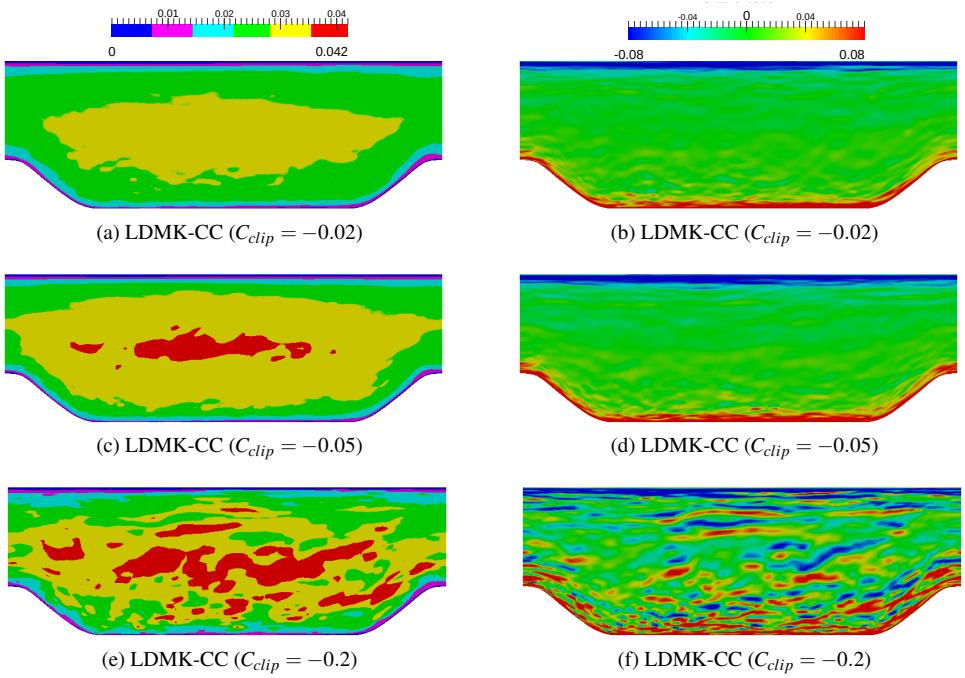

(a) LDMK-CC ($C_{clip} = -0.02$)

(b) LDMK-CC ($C_{clip} = -0.02$)

(c) LDMK-CC ($C_{clip} = -0.05$)

(d) LDMK-CC ($C_{clip} = -0.05$)

(e) LDMK-CC ($C_{clip} = -0.2$)

(f) LDMK-CC ($C_{clip} = -0.2$)

Figure 5: Contour plots of standard deviation of C_s (left plots) and gradient of standard deviation in y direction, $\partial \langle C_s' C_s' \rangle^{1/2} / \partial y$, for two stable LDMK-CC ($C_{clip} = -0.02$ and –0.05) and one unstable LDMK-CC ($C_{clip} = -0.2$) models. The time step for all simulations is $\Delta t = 0.002$.

is always stable for wide range of CFL number. It is found that the stress-realizibility condition ensures the stability of the model and without that the model can face with instability. The new stabilization method which was based on the realizibility of structure of SGS stress tensor can be easily extended to the other SGS models which are based on Boussinesq hypothesis. By applying the similar condition we made the original DSM model stable without any averaging. We performed extensive investigation on instability reasons originated from dynamic SGS models. For this end, we investigated the possible reasons such as: a) the frequencies of occurrence of local non-physical (non-realizable) events, b) effect of any correlation of model constant, c) imbalances originated by large fluctuations. We found that in contrast to Lund *et al.* (1993), instability does not occur due to long correlation of negative model constant. It occurs due to large gradients of standard deviation that happens in entire flow field.

ACKNOWLEDGMENTS

The authors would like to acknowledge support through NASA's NRA research opportunities in aeronautics program (Grant No. NNX12AJ71A) and the National Science Foundation (DMS - CDS&E-MSS, Grant No. 1622488, Technical Officer: Y. Zeng). We are very thankful for computational resources provided by the Advanced Research Computing Center and the Wyoming-NCAR Alliance at the University of Wyoming.

REFERENCES

Gopalan, H., Heinz, S. & Stöllinger, M. 2013 A unified RANS-LES model: Computational development, accuracy and cost. *Journal of Computational Physics* **249**, 249–274.

Heinz, S. 2003*a* On Fokker–Planck equations for turbulent reacting flows. Part 2. Filter density function for large eddy simulation. *Flow, Turbulence and Combustion* **70** (1), 153–181.

Heinz, S. 2003*b* *Statistical Mechanics of Turbulent Flows*, 1st edn. Springer-Verlag, Berlin, Heidelberg, New York, Tokyo.

Heinz, S. 2007 Unified turbulence models for LES and RANS, FDF and PDF simulations. *Theoretical and Computational Fluid Dynamics* **21** (2), 99–118.

Heinz, S. 2008 Realizability of dynamic subgrid-scale stress models via stochastic analysis. *Monte Carlo Methods and Applications* **14** (4), 311–329.

Heinz, S. & Gopalan, H. 2012 Realizable versus non-realizable dynamic subgrid-scale stress models. *Physics of Fluids* **24** (11), 115105/1–23.

Lund, T.S., Ghosal, S. & Moin, P. 1993 Numerical experiments with highly-variable eddy viscosity models. In *Proceedings of Engineering Applications of Large Eddy Simulations, FED ASME*, , vol. 162, pp. 7–11. New York.

Mellen, C. P., Frohlich, J. & Rodi, W. 2000 Large-eddy simulation of the flow over periodic hills. In *Proceedings of 16th IMACS world congress*, pp. 1–6. Lausanne, Switzerland.

Moin, P., Squires, K., Cabot, W. & Lee, S. 1991 A dynamic subgridscale model for compressible turbulence and scalar transport. *Phys. Fluids A* **28** (3), 2746.

Mokhtarpoor, R., Heinz, S. & Stoellinger, M. 2016 Dynamic unified rans-les simulations of high reynolds number separated flows. *Phys. Fluids* **28**, 095101.

Yoshizawa, Akira 1986 Statistical theory for compressible turbulent shear flows, with the application to subgrid modeling. *Phys. Fluids* **29**, 2152.